



Exosomal miR-199a-5p promotes hepatic lipid accumulation by modulating MST1 expression and fatty acid metabolism

Yuhan Li^{1,2,5} · Yansong Luan^{1,2} · Jianning Li^{1,2} · Hui Song^{1,2} · Yan Li^{1,2} · Hi Qi¹ · Bo Sun³ · Peng Zhang³ · Xianxian Wu⁵ · Xing Liu⁵ · Yanhui Yang^{1,2} · Wufan Tao⁴ · Lei Cai⁶ · Zhiwei Yang⁵ · Yi Yang^{1,2}

Received: 23 April 2020 / Accepted: 12 September 2020
© Asian Pacific Association for the Study of the Liver 2020

Abstract

Background and Aims Non-alcoholic fatty liver disease (NAFLD) and its complications has become an expanding health problem worldwide with limited therapeutic approaches. The current study was aiming to identify novel microRNA in the regulation of hepatic lipid metabolism in NAFLD.

Approches and Results Systematic screening of microRNA expression by high-throughput small RNA sequencing demonstrated that microRNA 199a-5p (miR-199a-5p) was significantly upregulated in high fat diet-induced steatosis mouse model, with the most abundant expression in adipose tissue. MST1 was further identified as the target gene for miR-199a with specific recognition at the 3' untranslated region with dual luciferase reporter assay. Delivery of miR-199a-5p with exosomes into mice aggravated liver lipid accumulation in hepatocytes, accompanied by down-regulation of hepatic MST1 expression and modulation of hepatic lipogenesis and lipolysis, including SREBP-1c, AMPK signaling cascades and the down-stream CPT1α and FASN. Conversely, administration of exosome containing anti-miR-199a-5p resulted in attenuated steatosis in mice fed on high fat diet. Importantly, miR-199a-5p-induced abnormal cellular lipid accumulation could be markedly reversed by overexpression of MST1.

Conclusion miR-199a-5p might be an essential regulator for hepatic lipid metabolism, possibly through its interaction with MST1 and the subsequent signaling cascade. Thus, miR-199a-5p may serve as an important therapeutic target in the treatment of NAFLD.

Keywords NAFLD · miR-199a-5p · Exosomes · MST1

Abbreviations

NAFLD	Non-alcoholic fatty liver disease
NASH	Non-alcoholic steatohepatitis
MST1	Mammalian sterile 20-like kinase 1

Electronic supplementary material The online version of this article (<https://doi.org/10.1007/s12072-020-10096-0>) contains supplementary material, which is available to authorized users.

Zhiwei Yang
yangzhiwei@cnilas.pumc.edu.cn

Yi Yang
yangyi0908666@163.com

¹ School of Basic Medical Sciences, Ningxia Medical University, Xingqing District, 692 Shengli St, Yinchuan 75004, China

² The Institute of Endocrinology, Ningxia Medical University, Yinchuan, China

³ Second Affiliated Hospital, Ningxia Medical University, Yinchuan, China

FASN	Fatty acid synthase
EXO	Exosomes
ACC	Acetyl-CoA carboxylase
CPT-1 α	Carnitine palmitoyltransferase I α
AMPK	AMP-activated protein kinase
PA	Palmitic acid
ORO	Oil red O

⁴ Institute of Developmental Biology and Molecular Medicine and State Key Laboratory of Genetic Engineering, School of Life Sciences, Fudan University, Shanghai, China

⁵ Institute of Laboratory Animal Science (ILAS), Chinese Academy of Medical Sciences and Peking Union Medical College (CAMS&PUMC), #5 Pan Jia Yuan Nan Li, Chaoyang District, Beijing 100021, China

⁶ Department of Physiology, Cardiovascular Research Center, University of Kentucky, Lexington, KY 40536, USA

TG	Triglycerides
EXO-miR	MiRNA-containing exosomes
sRNA-seq	High-throughput small RNA sequencing

Introduction

NAFLD is the most common chronic liver metabolic disorder which affects around 30% of the adult population [1–4]. The main pathogenic feature of the NAFLD is the accumulation of triglycerides in hepatocytes, normally resulted from the enhanced de novo lipogenesis and reduced lipid decomposition [5–7]. As NAFLD progressed from simple steatosis to non-alcoholic steatohepatitis (NASH), more severe liver damage occurs which featured hepatocyte cell death, ballooning and inflammation [8, 9]. The common risk factors of NAFLD and NASH include hyperlipidemia, diabetes and hypertension. In the past decades, therapeutic approaches have been focused on lowering the lipid load and enhancing insulin sensitivity, especially targeting on diglyceride acyltransferase [10], acetyl-CoA carboxylase (ACC) [11], fatty acid synthase (FASN) and AMP-activated protein kinase (AMPK) [12]. However, effective treatment is still unavailable for NASH apart from lifestyle intervention [5]. Therefore, elucidation of the molecular mechanism on the development of NAFLD and NASH is essential for the early prevention and delayed progression of the disease.

miRNAs are highly conserved non-coding RNA sequences, with 19–22 nucleotides in length, recognizing the target genes by complementary base pairing which eventually lead to their degradation or translational inhibition [13–15]. Recently, studies show that miRNA not only performs biological functions in its host cells, but can also regulate the biological functions of recipient cells via circulatory system [7, 16–20]. Exosomes, a nanoscale vesicle (30–100 nm) released by multiple cell types, serve as important carriers for protein and non-coding RNA into extracellular spaces or fluid to mediate cell–cell communication [18–20]. Such packaging of the miRNA within exosomal vesicles may increase miRNA stability and facilitate their delivery to distant sites in an intact state [7, 18, 21, 22]. Accumulating evidence indicates that adipose tissue expresses a wide variety of miRNA with relative high abundance [23]. Recent findings suggest that adipose tissue is a main source of circulating exosomal miRNAs, which can regulate gene expression in liver tissues and contribute to the progression of metabolic diseases [7, 21, 24, 25].

miR-199a-5p is highly expressed in breast, colon and testis while relatively low in liver and kidney [26]. The functions of miR-199a-5p have been extensively investigated in cancers. miR-199a-5p has been reported to modulate the expansion, proliferation and tumorigenic capacity in breast cancer, prostate cancer, gastric cancer and hepatocellular

carcinoma through targeting genes associated with mitogenesis and apoptosis, such as EGFR, aurora kinase A, YAP1 and ZHX1 [27–30]. miR-199a-5p is abundantly expressed in the adipose tissue where it functions to modulate obesity associated insulin resistance and inflammatory responses [31]. miR-199a-5p can be significantly upregulated by fatty acid, cytokines and adipokines [31]. However, the roles of miR-199a-5p in liver steatosis and NASH remain largely unknown.

A highly conserved serine/threonine kinase, mammalian sterile 20-like kinase 1 (MST1) is a core component of the Hippo signaling pathway that plays a pivotal role in regulating various cellular processes, including cell proliferation, immune responses, cell apoptosis, and autophagy [32–34]. The newly identified Hippo signaling is crucial for maintaining liver metabolic homeostasis and preventing the progression of NAFLD [35]. Previous study demonstrated that activation of PPAR γ by the MST1 signaling pathway may be a novel regulation mechanism for adipogenesis [36]. However, the molecular mechanism on MST1 in liver lipid metabolism remains elusive. In the current study, we demonstrated that hepatic MST1 can be regulated by adipose-associated miR-199a-5p which further impact the downstream AMPK and SREBP-1c signaling cascade. Thereby, miR-199a-5p might be a potential intervention for MST1 modulated hepatic lipid accumulation.

Materials and methods

Human liver specimens

Human liver specimens were collected from 11 patients (NON-NAFLD, $n=6$; NAFLD patients, $n=5$) admitted to Ningxia Medical University Second Affiliated Hospital (Yinchuan, China) for diagnosis and treatment of gallstone disease. Liver samples from the recruited subjects were obtained through needle biopsy. Patients with hepatitis B, hepatitis C, HIV infection are excluded from the study. Patients with history of smoking, alcoholic abuse or treated with lipid-lowering therapy were also excluded. NASH patients were diagnosed by ultrasound and pathological analysis of liver biopsy, defined by extensive steatosis, lobular inflammation, ballooning, formation of Mallory Denk bodies, and fibrosis [37, 38]. The NON-NAFLD control subjects were screened out from the patients diagnosed with gallstone who went through diagnostic liver biopsy with no pre-existing conditions (NAFLD, hepatitis, cirrhosis, and malignant tumors) (Suppl Fig. S6).

Reagents and materials

Dulbecco's modified Eagle's medium (DMEM), fetal bovine serum (FBS) penicillin/streptomycin, and Lipofectamine 2000 were supplied by Invitrogen (Carlsbad, CA, USA). Antibodies against MST1 (#3682), p-AMPK(Thr 172) (#2535), AMPK (#5831), p-ACC(ser79) (#3661), ACC (#3662) and p-SREBP-1c(Ser372) (#9874) were purchased from Cell Signaling (Danvers, MA, USA). SREBP1c (#14088-1-AP) were obtained from Proteintech (Wuhan, China). FASN (#Ab22759) and Anti-CD9 (ab92726) were obtained from Abcam (Cambridge, UK). Antibodies against actin (A5441) were purchased from Sigma (St. Louis, MO, USA). Anti-CD63 (sc-15363) was purchased from Santa Cruz Biotechnology (Dalla, TX, USA). The miR-199a-5p mimics, miR-199a-5p inhibitors and their respective negative control RNAs were purchased from RiboBio (Guangzhou, China).

Animal experiments

Male C57BL/6J mice used throughout the study were purchased from Beijing Vital River Laboratory Animal Technology Co., Ltd. (Beijing, China). For miR-199a-5p studies, 8-week old mice were fed NCD or HFD (60% kcal from fat, MD12033, Medi-science, China) for 12 weeks. Mice were then taken down following 8 h fasting while blood and tissue were collected. For MST1 studies, 8-week-old C57BL/6 mice fed on NCD or HFD for 12 weeks and then were i.v. injected with LV-shCtrl/LV-shMST1 ($n=8$) or LV-GFP/LV-MST1 for 7 days. Mice were then taken down and tissues were collected.

Cell culture and treatments

AML-12 (mouse liver cells) was acquired from ATCC (Manassas, VA, USA), and was maintained in DMEM medium supplemented with 10% FBS, 100 U/ml penicillin and 100 µg/ml streptomycin in a humidified atmosphere of 5% CO₂ at 37 °C. To determine the impact of gain and loss of function of miR-199a-5p, AML-12 cells were transfected with 2 µg exosomes containing either 100 nM of miR-199a or anti-miR-199a for 24 h, followed by treatment with 250 µM palmitic acid (PA) (Sigma, St. Louis, MO, USA) for additional 12 h.

Luciferase reporter assay

AML-12 cells were co-transfected with 100 nM of mimics control or miR-199a together with 50 ng of pmirGLO (dual-luciferase reporter plasmid) that contained 3'-UTR of target gene for 48 h. Luciferase activity was then determined by Dual Luciferase Reporter Assay System (E2920, Promega,

Madison, WI) using a Centro LB 960 (BERTHOLD, Germany).

Isolation and detection of mRNA and miRNA

Total RNA was isolated from exosomes using TRIzol® LS Reagent following the manufacturer's protocol (Invitrogen, Carlsbad, CA, USA). Subsequently, 100–500 ng of RNA was subjected to reverse transcription into cDNA using the PrimeScript™ II 1st Strand cDNA Synthesis Kit (#6210A, TaKaRa, Japan). Real-time PCR was then performed using TB Green™ Premix Ex Taq™ II (TliRNaseHPlus, #RR820A, TaKaRa, Japan) on Applied Biosystems Step One Plus Real-Time PCR System (Thermo Fisher Scientific, Waltham, MA, USA). For target mRNA gene expression, data were normalized to β-actin levels while for micro-RNA determination, data were normalized to U6 levels. The 2-ΔΔCT method was used to determine the relative RNA expression. Primer information was listed in supplementary Table S1 & S2.

High-throughput small RNA sequencing (sRNA-seq) and bioinformatics analysis

Total RNA was extracted from mouse liver and adipose tissue using TRIzol® Reagent according to the manufacturer's protocol. RNA quality was assessed using RNA Nano 6000 Assay Kit of the Agilent Bioanalyzer 2100 system (Agilent Technologies, CA, USA). miRNA sequencing libraries were generated using the NEBNext® Multiplex Small Library Prep Set for Illumina® (NEB, USA) following manufacturer's instruction. The library quality was assessed on the Agilent Bioanalyzer 2100 system using DNA High Sensitivity Chips. Quantification of miRNA expression levels was determined by TPM (per million transcriptions). TruSeq SR Cluster Kit v3-cBot-HS (Illumia) was used to cluster the index-coded samples and DESeq R package (1.8.3) was adopted to analyze the differential expression of two conditions/groups. The *p* values were adjusted using the Benjamini and Hochberg method. Corrected *p* value of 0.05 was set as the threshold for significantly differential expression by default. Differential miRNAs were screened from two levels, i.e., fold change and corrected significance level (padj/qvalue) to infer the overall distribution of differential miRNAs, as indicated in volcano map. Sequencing data supporting these studies can be found at the Gene Expression Omnibus database under accession number GSE97652. For miRDB analysis (<https://www.mirdb.org>), a search by target gene was performed against the mouse database. A target score of 75 was set to exclude potential false-positive interacting miRNAs.

Exosome isolation and quantification

Exosomes were isolated from the conditioned medium (CM) of HEK293 cells. Briefly, HEK293 cells were grown in DMEM supplemented with 10% exosome-depleted FBS. Supernatant was obtained by successive centrifugation at 300×g for 10 min (4 °C), 2000×g for 30 min (4 °C) and 10,000×g for 1 h (4 °C), and ultracentrifuge at 120,000×g (4 °C) for 6–8 h in a S110AT rotor in a Sorvall MTX 150 ultracentrifuge (Thermo Fisher Scientific, Waltham, MA, USA). Pellets were resuspended in PBS and ultra-centrifuged again at 120,000×g for 20 min (4 °C). The pellets were resuspended in 100 µl PBS and the protein content of exosomes was determined by BCA protein assay reagents (KeyGen BioTech, China). Proteins were further separated by 10% SDS-PAGE and transferred to a PVDF membrane (Thermo Fisher Scientific, Waltham, MA, USA). Exosome-associated protein markers anti-CD63 and anti-CD9 were measured by immunoblotting to further characterize the exosome property. The number and size of particles in exosomes were measured by Zeta View PMX110 instrument at 405 nm wavelength. Photos were taken at 30 frames per second for 1 min. NTA software (ZetaView8.02.28) was used to analyze the movement of particles to verify the purity of exosomes.

Electron microscopy

Exosome specimens for TEM characterization were placed onto copper mesh form vargrids (Electron microscopy Sciences, Hatfield, PA, USA) for 10 min. Afterwards, the residual liquid was sucked away from the edge of the copper mesh with a filter paper. The sample was stained by 2% phosphotungstic acid for 10 min. Samples were observed using a H7650 transmission electron microscope (Hitachi, Tokyo, Japan) operated at an accelerating voltage of 80 kV. Images were taken with an AMT digital camera for data acquisition.

Package miRNAs into exosomes

A XMIRXpress expression lentivectors (#XMIRXP-Vect, System Biosciences, CA, USA), which can specifically encapsulate miRNAs into exosomes, were used to deliver miR-199a-5p. Briefly, XMIR-miR-199a or XMIR-miR-NT lentiviruses were generated according to manufacturer's instructions (Invitrogen, Carlsbad, CA, USA). These lentiviral vectors were then transfected into HEK293 cells for 48 h. Exosomes were then isolated from the HEK293 cells supernatant by ultracentrifugation. Exosome features were further characterized by detecting the specific exosomal protein by western blot analysis and electron microscopy. miR-199a-5p of exosome was determined by real-time PCR.

Exosome trafficking in vitro by fluorescence microscopy

HEK293 cells were transfected with XPack-RFP (#XPA-K120PA-1, System Biosciences) vector for 24 h using Lipofectamine 2000 (Invitrogen, Carlsbad, CA, USA). 48 h post-transfection, XPack exosomes were isolated and incubated with AML-12 mouse liver cells for additional 24 h which were further subjected to fluorescence microscopy analysis (BX51, Leica).

Exosome trafficking in vivo by FLECT/CT

Fluorescence emission tomography (FLECT) imaging was performed using the Trifoil InSyTe FLECT® imager (Tri-Foil Imaging, Chatsworth, CA, USA). The nude mice with exo-miR-199a-5p injection were anesthetized by isoflurane (4% for induction, 1.5% for maintenance in 30% oxygen and 70% nitrous oxide) and images of three-dimensional acquisition with 730 nm excitation laser and 803 nm filter were obtained. The absorption data were collected at 29 slices with 1 mm spacing and 29 source angles per slice. Reconstruction of FLECT image was performed using 1 mm 3 grid with attenuation correction and 1000 iterations to generate the reconstructed three-dimensional image of each scan. Following the FLECT scan, the computed tomography (CT) scan was performed for each animal using X-ray voltage of 45 kVp, exposure time of 1500 ms and over 360° projections to generate FLECT image, which was overlayed onto its respective FLECT image. Image files of FLECT and CT scan were then co-registered, fused, analyzed and quantified (In Vivo Scope version 2.00).

Statistics

All results are expressed as the mean ± SEM. The differences between two groups were analyzed by Students' *t* test, while the difference between two more groups were analyzed by one-way ANOVA followed by post-Tukey test (SPSS 21). *p* values less than 0.05 were considered significant.

Results

miR-199a-5p is highly expressed in mouse adipose tissue and interfere with the liver lipid metabolism

NAFLD mouse models were generated by high fat feeding while the relevant miRNAs were identified by deep sequencing of small RNAs. A total of 1000 miRNAs were detected in adipose tissue. As shown in Fig. 1a, the miRNA heat map revealed that a total of 252 miRNA were differentially expressed in adipose tissue of mice fed on

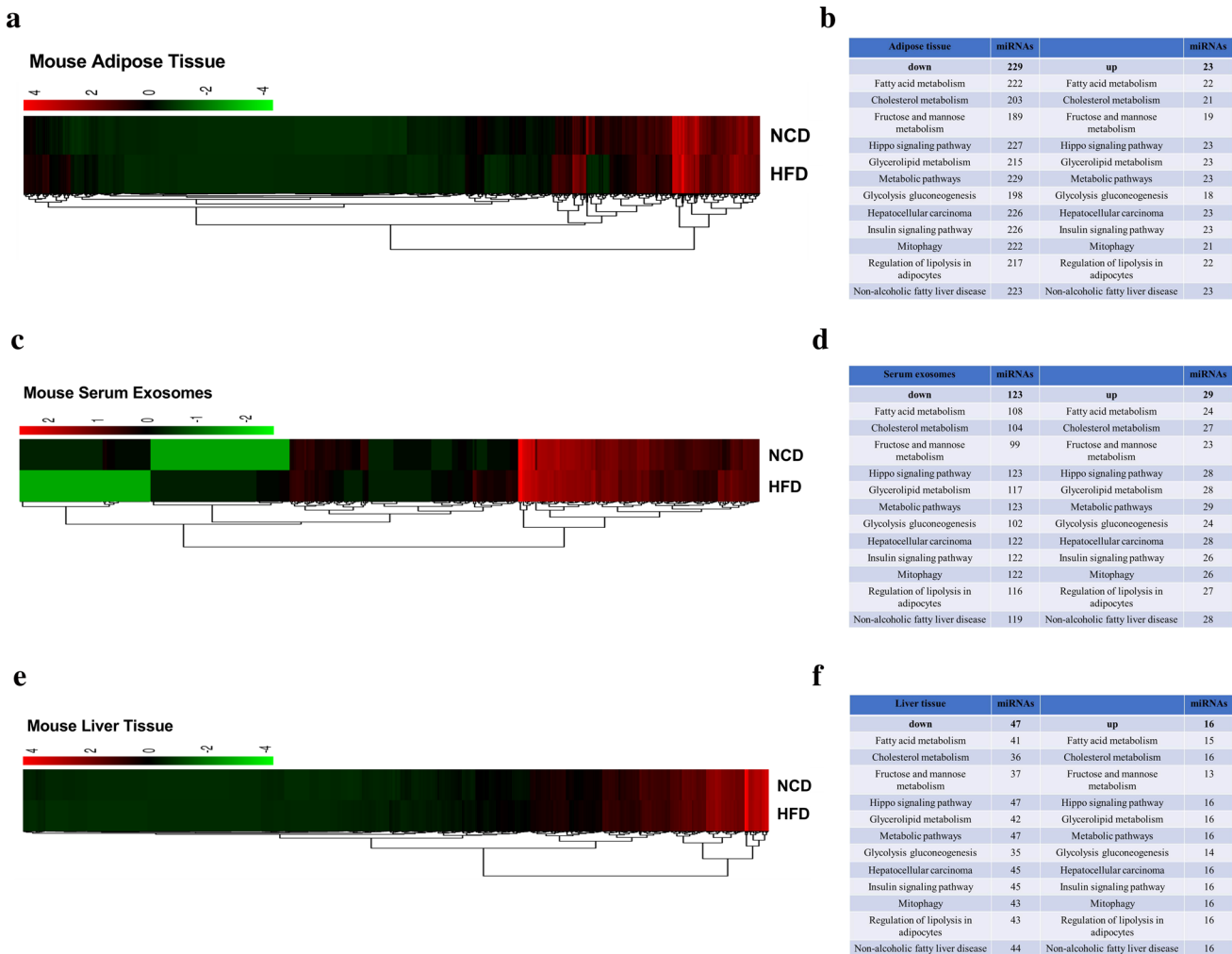


Fig. 1 Expression profile of miRNA in mouse adipose tissue, serum exosomes and liver tissue. Plasma and tissues were harvested from control and NAFLD mice. Total RNA was subjected to microRNA microarray analysis on the Agilent mouse genome microRNA array. The heat map shows differentially expressed miRNAs in HFD and control mice. Red indicates upregulated microRNAs, and green re-

normal chow diet (NCD) and high fat diet (HFD). Among those miRNAs, 23 miRNAs were significantly upregulated in adipose tissue, especially miR-199a-5p (Suppl Pic. 1). DIANA-microT, miRNAPath, and miRWalk analyses further revealed that most of the upregulated miRNAs in adipose tissue were involved in the regulation of lipid metabolism (Suppl Pic. 2 and Fig. 1b). Similar experimental approaches were applied to identify the differentially expressed miRNAs in serum exosomes and liver tissues. In HFD fed mice, a total of 152 miRNAs were differentially expressed in exosomes from serum (Suppl Pic. 3 and Fig. 1d), with 29 miRNAs upregulated while 63 miRNAs were differentially expressed in liver, with 16 miRNAs upregulated (Suppl Pic. 4 & Fig. 1f). As observed in adipose tissue, a large portion of those differentially

resent down-regulated miRNAs for more than two-fold ($p < 0.05$). **a**, **b** Heat map and table showing differentially expressed miRNAs in adipose tissue. **c**, **d** Heat map and table showing differential express miRNAs in mouse serum exosome. **c** Heat map and table showing differentially expressed miRNAs in mouse liver tissue

expressed miRNAs was targeting the lipid metabolism pathways.

The tissue distribution of miR-199a-5p was further explored by deep sequencing of small RNAs in serum exosomes and liver tissues. Volcanic map analysis further confirmed that miR-199a-5p is highly expressed in adipose tissue (Fig. 2a). The miR-199a expression in various tissues of mice on NCD or HFD was further verified by real-time PCR analysis, which confirmed that miR-199a-5p is most abundantly expressed in adipose tissue (Fig. 2b). In contrast to the high abundance in adipose tissue, miR-199a expression is relatively low in serum exosomes and liver tissues (Fig. 2b).

To further elucidate the function of miR-199a-5p in liver lipid storage, we transfected AML-12 mouse liver

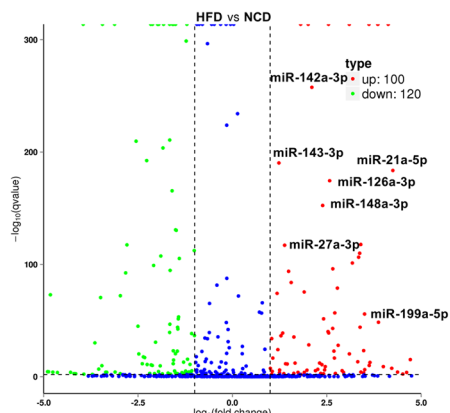
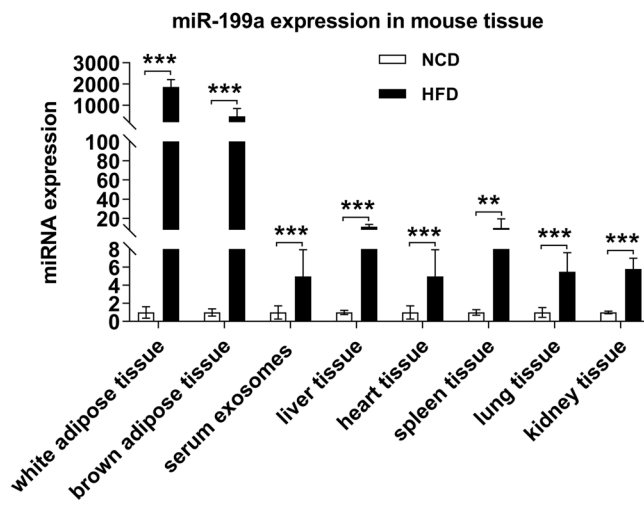
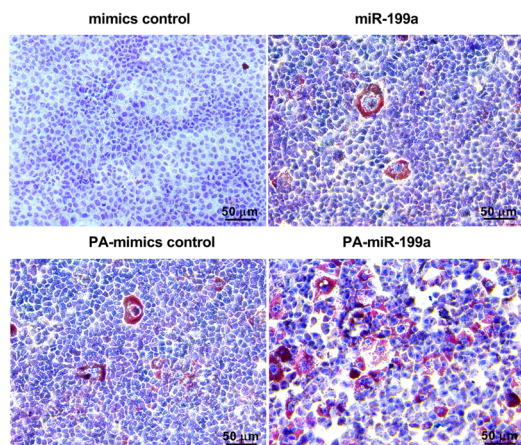
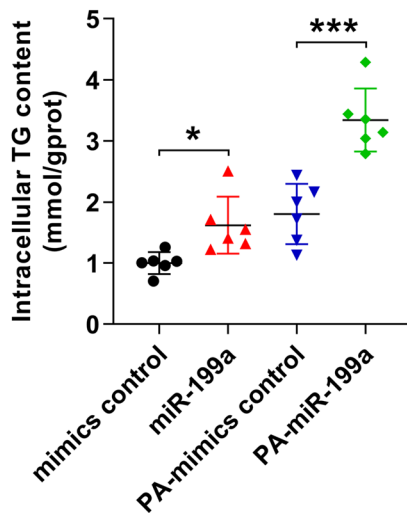
a**b****c****d**

Fig. 2 miR-199a-5p is mainly distributed in adipose tissue and can aggravate liver lipid accumulation. C57BL/6 mice were fed on HFD or NCD for 12 weeks after which mice were taken down, while blood and tissue were collected. **a** Volcano plot showing miR-199a-5p is markedly upregulated in mouse adipose tissue in response to HFD. **b** miR-199a-5p tissue distribution in mice fed on HFD or NCD ($n=12$).

c, d AML-12 cells transfected with miR-199a-5p in the absence or presence of PA. Cellular lipid accumulation was determined by ORO staining (c) and intracellular TG content (d). Scale bar 50 μ m. Data are expressed as the mean \pm SEM ($n=3$ per group). * $p<0.05$, ** $p<0.01$, *** $p<0.001$.

cells with miRNA mimics control or miR-199a-5p mimics in the absence or presence of Palmitic acid (PA). As illustrated by the Oil red O (ORO) staining, a significant increase in lipid accumulation was observed in liver from miR-199a-5p groups than control group (Fig. 2c). In consistent, hepatic intracellular triglyceride (TG) content was also markedly higher in miR-199a-5p transfected group compared with the control group (Fig. 2d). These results demonstrate that miR-199a-5p promotes liver fat accumulation.

Exosome miR-199a-5p secreted by HEK293 cells aggravates liver lipid droplet formation

It has been shown that miRNAs can be efficiently transported from the adipose tissue to the distant target tissues to exert their functions via exosomes. Therefore, despite the relatively low expression level in the liver, miR-199a-5p could still function to regulate the hepatic metabolic conditions. Initial experiment was designed to

address whether distant miR-199a-5p could be transported to the liver and modulated hepatic lipid metabolism.

Exosomes (EXO) are miRNA-containing extracellular vehicles (EVs) secreted from various cells [19]. Circulating exosome is known to be a primary carrier of miRNAs [18]. The initial in vitro experiment confirmed that exosomes secreted by HEK293 cells can successfully transported to AML-12 cells (Suppl Fig. S1C, D). In this study, XMIRX expressing lentiviral vectors miR-199a-5p (XmiR-199a) or

XMIRX expressing non-targeting miRNA (XmiR-NT) lentiviral vectors were used to package miRNAs into exosomes which were subsequently harvested by differential ultracentrifugation. As indicated in immunoblotting, the levels of exosome-associated protein markers CD9 and CD63 were much higher in the EXO treated group compared to the untreated HEK293 group (Fig. 3a). Electron microscopy revealed that particles isolated by ultracentrifugation contain abundant HEK293-derived EXO with a diameter of

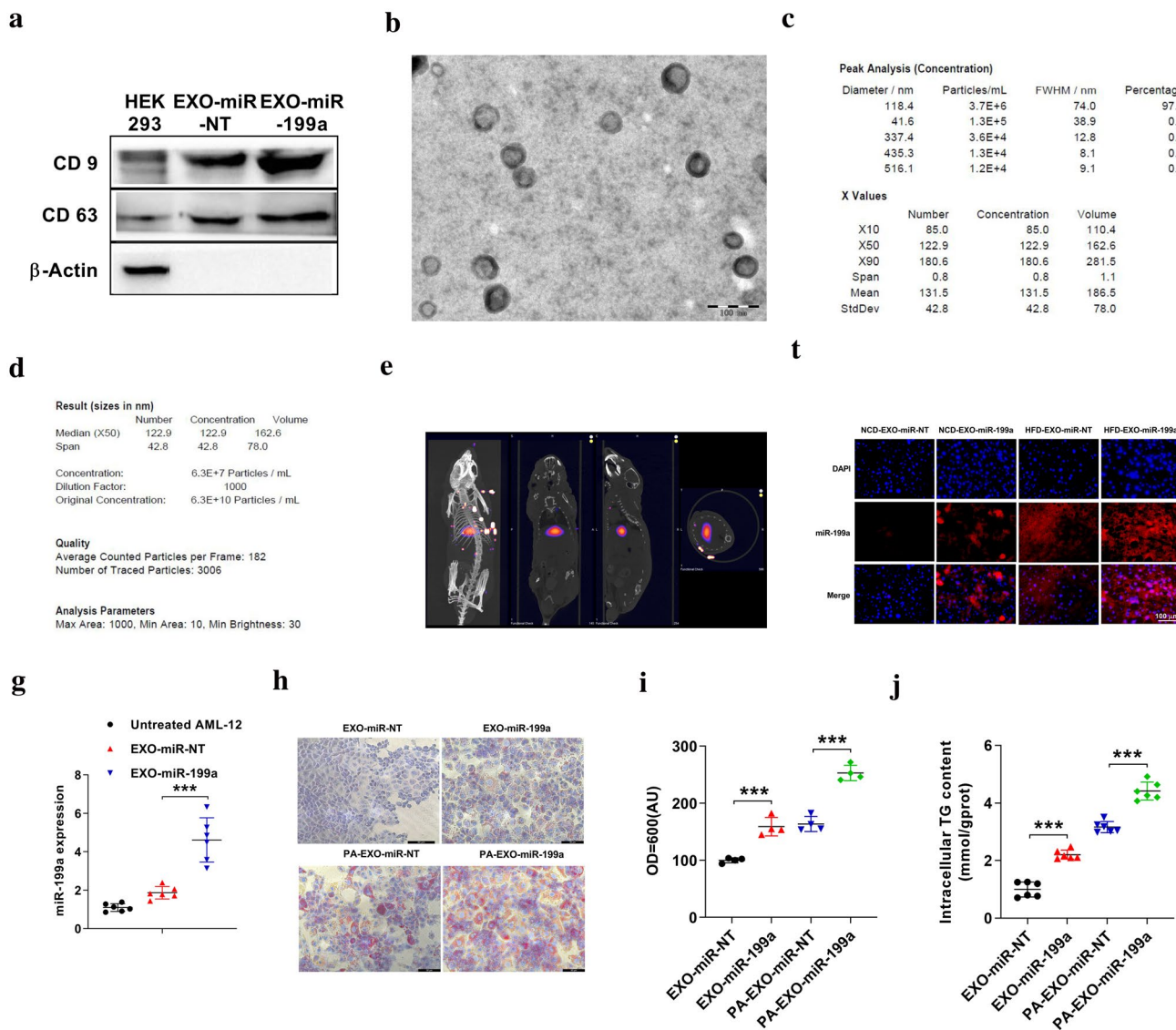


Fig. 3 Characterization of the exosomal miRNA. **a** Exosome-associated protein markers CD63, and CD9 were measured by western blot analysis using commercially available antibodies. **b** Electron microscopy analysis of exosomes secreted by HEK293 cells. Scale bar 100 nm. **c**, **d** The exosomal particle concentration (**c**) and size (**d**) were determined by the Zeta View PMX110 instrument. **e** Nude mice were i.v. injected with targeting-fluoroprobe (Targ-GFP) and images were obtained by FLECT/CT scanning. Pictures shown are representative maximum intensity projection of FLECT/CT images of Targ-

GFP mice. **f** RNA fluorescence in situ hybridization. Blue, nucleus; Red, miR-199a. Scale bar 100 μ m. **g–j** AML-12 mouse liver cells were exposed to the EXO-miR-199a for 48 h in the absence or presence of PA. The levels of miR-199a-5p was demined by quantitative real-time PCR. The relative gene expression was normalized to U6 level (**g**). Neutral lipids accumulation was determined by ORO staining (**h**, **i**) and TG levels were determined by enzymatic analysis (**j**). Scale bar 50 μ m. Data are expressed as the mean \pm SEM ($n=6$ per group). * $p < 0.05$, ** $p < 0.01$, *** $p < 0.001$

30–100 nm (Fig. 3b). The purity of the exosomes was further confirmed by examining the nanoparticle size from the extracted exosomes. As shown in Fig. 3c, d, the concentration of exosomes secreted by HEK293 was 6.2×10^{10} and the average particle size was 117.3 (nm), indicating high purity and yield of the exosomes.

The transportation of exosome was measured by determining the in vivo GFP-labeled EXO-miR-199a distribution in mice. Impressively, EXO-miR-199a-treated mice displayed a significantly higher circulating and hepatic miR-199a-5p expression (Suppl Fig. S1A, B), with the majority of miR-199a-5p distributed to the mouse liver (Fig. 3e). RNA fluorescence in situ hybridization analysis further indicates miR-199a-5p expression is significantly higher in EXO-miR-199a group than in EXO-miR-NT (Fig. 3f). Results obtained from the above experiments indicate that miR-199a containing exosomes secreted from HEK293 cells can be delivered to liver.

To investigate the effect of EXO-miR-199a on hepatic lipid droplet formation, we directly added EXO-miR-199a or EXO-miR-NT to AML-12 mouse liver cells in the absence or presence of PA. The expression of miR-199a-5p in the EXO-miR-199a group was several folds higher than that in the EXO-miR-NT group by qPCR (Fig. 3g). ORO staining and quantification showed that lipid accumulation and the intracellular triglyceride content were markedly increased in EXO-miR-199a group compared with EXO-miR-NT group (Fig. 3h–j). Taken together, we conclude that miR-199a-5p, which highly expressed in adipose tissue, can be transported to the liver through exosomes and might be associated with the hepatic lipid droplet formation.

EXO-miR-199a-5p interferes with liver lipid metabolism by inhibiting hepatic MST1 expression

To further elucidate the molecular mechanism of miR-199a-5p function, we explore the potential target of miR-199a which modulates hepatic lipid metabolism. MST1, an important regulator for lipid metabolism, has been identified as miR-199-5p target gene. The interaction of miR-199a and MST1 was determined in AML-12 mouse liver cells by Dual-Luciferase reporter assay. AML-12 mouse liver cells transfected with miR-199a-5p showed significant down-regulation of MST1 3'UTR luciferase activity both in the absence or presence of PA (Fig. 4a, b). Of note, in NAFLD patients, miR-199a-5p level was negatively correlated with the mRNA levels of hepatic MST1 (Fig. 4c). Such effect indicates that miR-199a-5p might be impact the progression of NAFLD, possibly through modulating the MST1 expression.

The protective role of MST1 in the regulation of liver lipid metabolism has been confirmed in both in vitro and

in vivo experiments (Suppl Fig. S2, S3, S4). MST1 expression was substantially down-regulated in mice fed on HFD compared to NCD (Suppl Fig. S2B). Similar down-regulation of MST1 was also observed in human NAFLD patients (Suppl Fig. S2D) and lipid loaded AML-12 cells (Suppl Fig. S2F). The down-regulation of MST1 in lipid overloading conditions is accompanied by alterations in hepatic lipid metabolism, as featured by decreased lipid mobilization (down-regulation of SREBP-1c, AMPK and ACC expression) and increased fatty acid synthesis (up-regulation of FASN) (Suppl Fig. S2A, C, E).

In HFD-induced steatosis mouse model, sh-MST1-mediated silencing of MST1 gene expression resulted in a substantial elevation of circulating and hepatic total cholesterol and triglycerides levels than that of control mice (Suppl Fig. S3A, C). Similar results were also observed in mice fed an NCD (Suppl Fig. S3B). In consequence, silencing of MST1 gene expression also induced the hepatic fatty acid synthesis while inhibiting hepatic fatty acid mobilization, as indicated by elevated FASN protein expression together with decreased p-SREBP-1c, p-AMPK and p-ACC expression (Suppl Fig. S3D). Such impact also occurred in lipid loading conditions. In AML-12 cells treated with PA, attenuation of MST1 expression also impacted the cellular lipid accumulation and fatty acid metabolism (Suppl Fig. S3E, F, G). Conversely, in steatosis mouse model and lipid loaded hepatocyte, over-expression of MST1 by lentiviral vector led to reduced cellular lipid accumulation (Suppl Fig. S4), accompanied by enhanced mobilization of fatty acid and subdued fatty acid synthesis, with increased phosphorylation of SREBP-1c, AMPK, ACC and decreased FASN expression (Suppl Fig. S4).

Furthermore, in the absence of PA, expression of EXO-miR-199a in AML-12 cells results in an inhibition of MST1 protein expression as determined by immunoblotting. Meanwhile, phospho-SREBP-1c, phospho-AMPK and phospho-ACC protein expressions were also significantly decreased, and FASN protein expressions were increased (Fig. 4d). In consistent, EXO-miR-199a expression also inhibited the gene expression of MST1 and a lipolysis-related gene (CPT-1 α) while upregulated lipogenesis-related gene (FASN) (Fig. 4e). Similar alterations in MST1, SREBP-1c, AMPK, ACC, FAS mRNA and protein expression were observed in EXO-miR-199a expressing cells treated with PA (Fig. 4f, g). Therefore, EXO-miR-199a might modulate cellular lipid metabolism through targeting MST1 and the downstream SREBP-1c and AMPK signaling cascade which subsequently stimulate the fatty acid synthesis and inhibit the lipolysis pathway, which ultimately leads to cellular lipid accumulation.

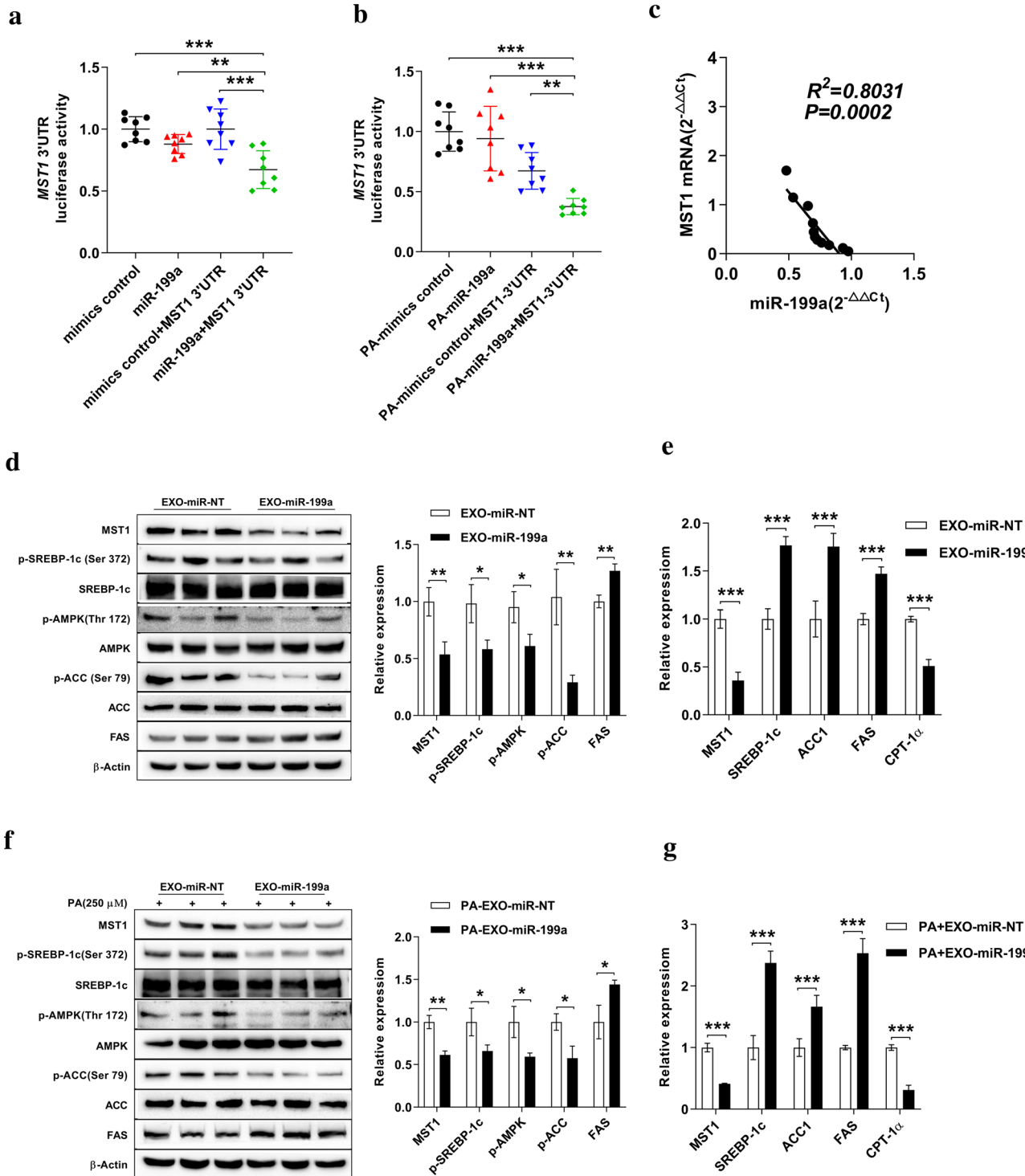


Fig. 4 EXO-miR-199a could promote lipid accumulation by targeting MST1 3'UTR region in AML-12 cells. **a, b** AML-12 cells were incubated with MST1 3'UTR luciferase reporter, mimics control or miR-199a-5p for 48 h in the absence (**a**) or absence (**b**) of PA. Luciferase activity of MST1 3'UTR was determined by dual luciferase reporter system ($n=4$). **c** miR-199a-5p and mRNA levels of hepatic MST1 were measured by q-PCR in NAFLD patients. A significant negative correlation was observed between miR-199a-5p and hepatic MST1 as analyzed by linear regression ($n=5$). **d–g** AML-12 mouse liver cells

were exposed to the EXO-miR-199a for 48 h in the absence (**d, e**) or presence (**f, g**) of PA. Cellular protein was extracted and target protein (MST1, AMPK, SREBP, ACC, FAS) expression was determined by immunoblotting. The relative protein expression was quantified by densitometry and normalized to β -actin expression level (**d, f**). mRNA expression was determined by q-PCR and was normalized to GAPDH levels (**f, g**). Data are expressed as the mean \pm SEM ($n=3$). * $p<0.05$, ** $p<0.01$, *** $p<0.001$

EXO-miR-199a-5p promotes liver fat accumulation in vivo

The impact of EXO-miR-199a on hepatic lipid metabolism was further tested in vivo. EXO-miR-199a-treated mice, either on NCD or HFD displayed a markedly elevated hepatic triglyceride production and accumulation as indicated by ORO and H&E staining (Fig. 5a). Liver weights, plasma triglycerides, and liver lipid contents were also significantly increased in the EXO-miR-199a-treated mice compared to the EXO-miR-NT mice (Fig. 5b–e). Interestingly, in mice treated with EXO-miR-199a, either on HFD or NCD diet, a significant reduction of MST1 gene expression was observed in the liver (Fig. 5f). To further explore the molecular mechanism of EXO-miR-199a function, we examined pathways associated with lipid metabolism by measuring the hepatic target protein expression. Consistent with the in vitro experiments, EXO-miR-199a expression also showed decreased phosphorylation of SREBP-1C, AMPK and ACC1 and increased FASN protein expression in liver (Fig. 5g). RT-qPCR screening on genes related to fatty acid and TG synthesis further confirmed the impact of EXO-miR-199a on liver lipid deposition. As indicated, a substantial up-regulation of genes associated with fatty acid synthesis (ACC, FASN, SREBP-1c), together with genes associated with TG synthesis (PPAR γ , LXR α , DGAT2) were observed in EXO-miR-199a mice compared with EXO-miR-NT mice (Fig. 5h).

EXO-anti-miR-199a ameliorate liver steatosis in vitro and in vivo

The impact of miR-199a-5p in hepatic lipid accumulation was further evaluated in a series of loss of function studies. For in vitro studies, AML-12 cells were transfected with negative control or EXO-miR-199a inhibitor in the presence of PA (Suppl Fig. S5A). In contrast to the EXO-miR-199a overexpression models, AML-12 cells treated with anti-miR-199a demonstrated a significant reduction in intracellular lipid accumulation compared with control cells, as reflected by decreased intracellular TG content and lipid levels (Fig. 6a–c). Target proteins related to the pathways of lipid metabolism were further evaluated. As indicated, anti-miR-199a-treated cells displayed no inhibition of MST1 gene expression, and meanwhile, enhanced phosphorylation of SREBP-1C, AMPK and ACC1 as well as down-regulated FASN protein expression (Fig. 6d, e). Moreover, the expression levels of lipogenic genes were also dramatically decreased in cells transfected with anti-miR-199a compared with cells transfected with control vector (Fig. 6f).

To investigate the effect of inhibition of miR-199a on fat accumulation in vivo, we administrated negative control or EXO-anti-miR-199a into HFD-induced C57BL/6J

mice through the tail vein injection (Suppl Fig. S5B). As expected, fat accumulation decreased dramatically in livers of HFD mice treated with EXO-anti-miR-199a (Fig. 7a). Strikingly, the livers of EXO-anti-miR-199a treated mice weighed much less compared with those from EXO-NC-inhibitor treated mice (Fig. 7b). Anti-miR-199a treatment also induced significant reduction in liver steatosis, demonstrated by the decreased contents of hepatic and serum TG and cholesterol (Fig. 7c–e). The MST1 expression and alterations in target protein expression associated with lipid metabolism pathways in liver of EXO-anti-miR-199a treated mice were consistent with results obtained in loss of function of miR-199-5p in AML-12 cells (Fig. 7f, g). Using RT-qPCR to detect liver lipogenic genes, we found that genes associated with TG synthesis as well as fatty acid synthesis and transport were down-regulated in EXO-anti-miR-199a mice compared to EXO-NC-inhibitor mice (Fig. 7h). Taken together, our results indicate that the loss of miR-199a-5p function by the application of anti-miR-199a-5p decreases lipogenic gene expression and prevent hepatic steatosis in HFD mice.

Overexpression of MST1 could reverse the miR-199a-5p mimics-induced lipid accumulation

Previous studies have shown that miR-199a-5p resulted in increased expression of lipogenic genes in liver and contributed to the development of steatosis. The impact of miR-199-5p in hepatic lipid metabolism is likely to function through MST1. To test our hypothesis, we stimulated the MST1 expression by lentiviral vector in AML-12 transfected with miR-199a-5p mimics in the absence or presence PA. ORO staining (Fig. 8a, b) and intracellular TG determination (Fig. 8c), both showed that overexpression of MST1 can reverse the miR-199a-5p mimics-induced lipid accumulation. Accordingly, enhanced phosphorylation of SREBP-1C, AMPK and ACC1 as well as down-regulated FASN protein expression was also observed in MST1 treated cells (Fig. 8d–f). Overall, these data suggest that miR-199a-5p can aggravate fatty liver disease by inhibiting the expression of MST1 (Fig. 9).

Discussion

The current study revealed for the first time that miR-199a-5p modulates the disease progression of NAFLD through targeting MST1. Through systematic screening, we identified that miR-199a-5p is highly expressed in adipose tissue and is correlated with the NAFLD. Overexpression of miR-199-5p promotes hepatic lipid accumulation through modulation of lipogenesis and lipolysis. In contrast, inhibition of miR-199-5p by the introduction of anti-miR-199-5p

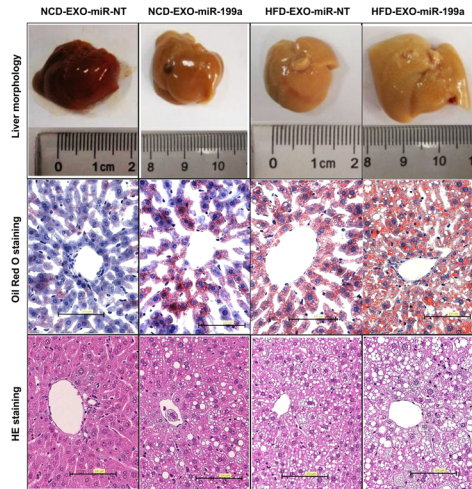
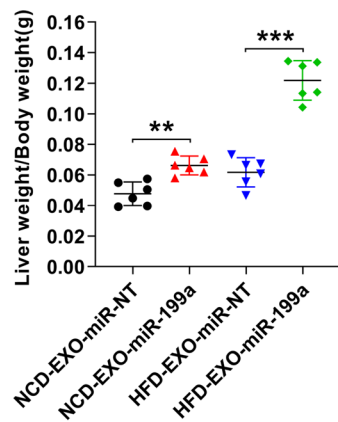
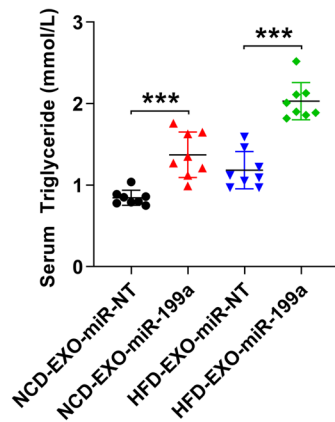
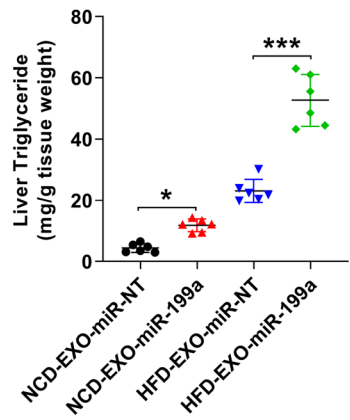
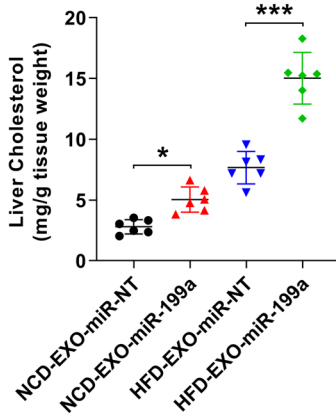
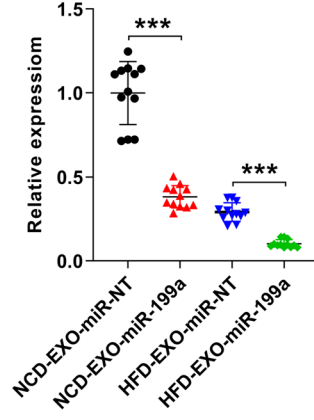
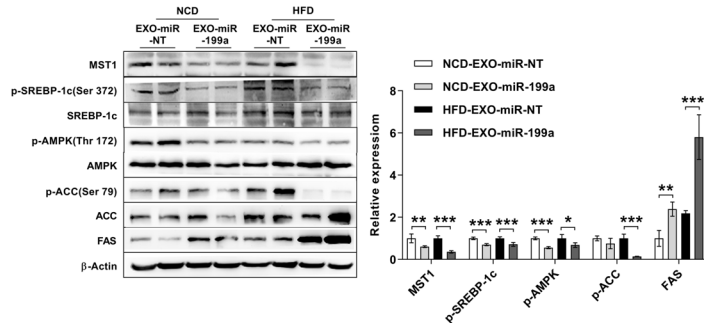
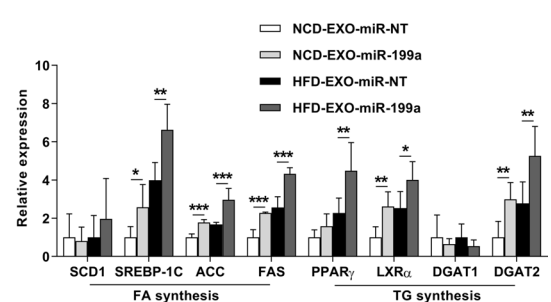
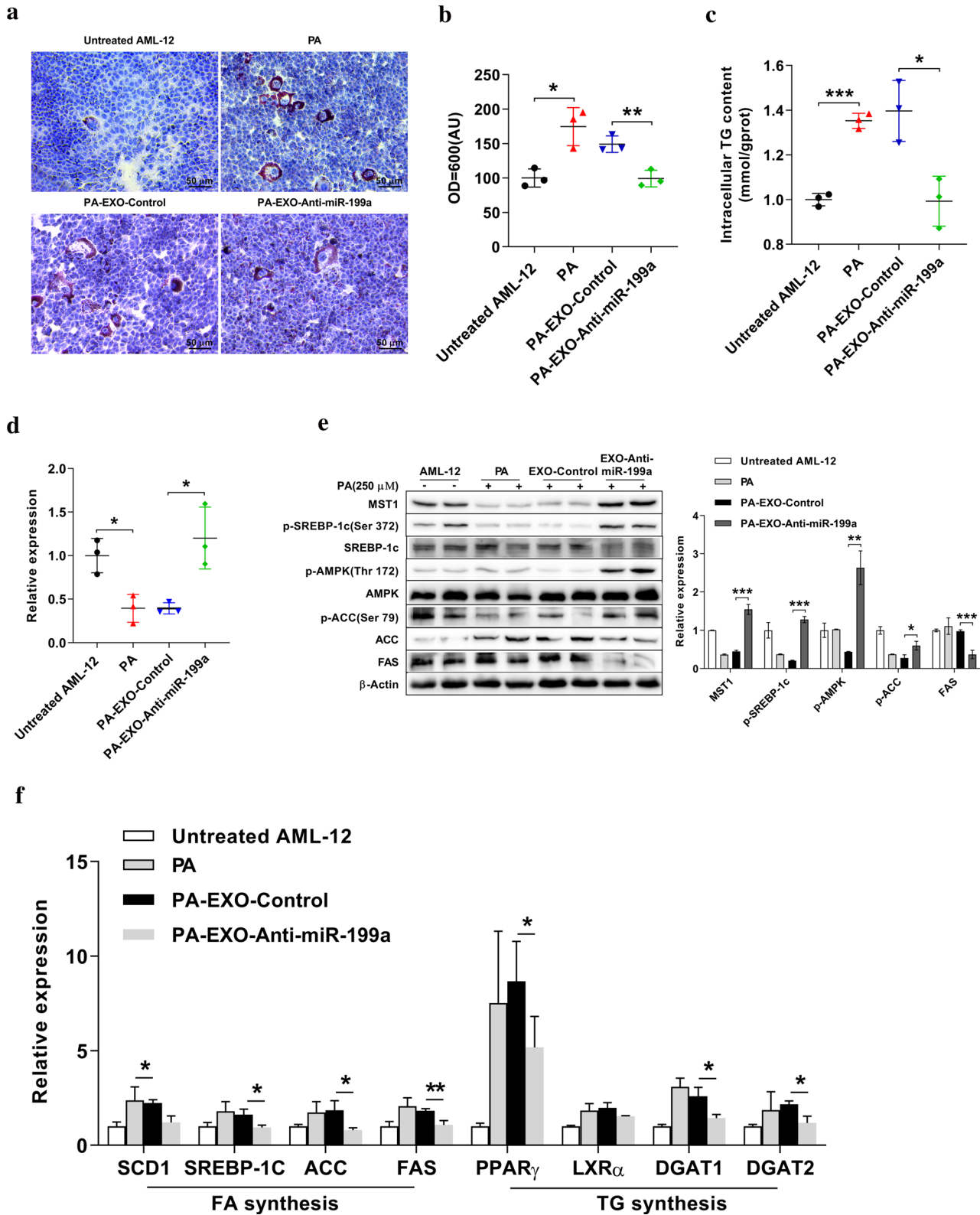
a**b****c****d****e****f****g****h**

Fig. 5 EXO-miR-199a significantly increased imbalance of liver fatty acid metabolism. **a–h** Mice were fed on NCD or HFD for 12 weeks and then were injected through the tail vein with 30 µg exosomes containing either a negative control (miR-NT) or miRNA mimics (miR-199a) bi-weekly for three additional weeks. Mice were taken down and blood and liver were collected. **a** Representative liver tissue sections with ORO and H&E staining. Scale bar 200 µm. **b** Fresh liver weight in each group. Data are expressed as the mean ± SEM ($n=6$). **c–e** Plasma and liver lipid contents as determined by commercial available kits ($n=6$). **c** Plasma TG levels. **d** Liver TG levels. **e** Liver cholesterol levels. **f** Hepatic MST1 mRNA level. The mRNA levels were measured by q-PCR ($n=6$). **g** Immunoblotting analysis of target protein expression using commercially available antibodies. The relative expression was determined by densitometry and normalized to β-actin levels. **h** The mRNA levels of lipid-related genes were measured by q-PCR and normalized to GAPDH expression level. Data are expressed as the mean ± SEM ($n=6$). * p < 0.05, ** p < 0.01, *** p < 0.001

cially available kits ($n=6$). **c** Plasma TG levels. **d** Liver TG levels. **e** Liver cholesterol levels. **f** Hepatic MST1 mRNA level. The mRNA levels were measured by q-PCR ($n=6$). **g** Immunoblotting analysis of target protein expression using commercially available antibodies. The relative expression was determined by densitometry and normalized to β-actin levels. **h** The mRNA levels of lipid-related genes were measured by q-PCR and normalized to GAPDH expression level. Data are expressed as the mean ± SEM ($n=6$). * p < 0.05, ** p < 0.01, *** p < 0.001



markedly ameliorates the hepatic lipid accumulation and steatosis. MST1 was further identified as a target gene for miR-199a-5p with specific recognition at the 3' untranslated

region. Overexpression of miR-199a-5p led to a down-regulation of hepatic MST1, accompanied by enhanced accumulation of lipid droplets in the liver. Such effects

◀Fig. 6 EXO-miR-199a inhibitor inhibits fat accumulation in vitro. AML-12 cells were transfected with EXO-miR-199a inhibitor and treated with PA. **a** The lipid content in AML-12 cells was determined fluorimetrically using ORO. Scale bar 50 μ m. **b** Quantitative results of ORO staining. **c** TG levels were determined by enzymatic analysis. **d** MST1 mRNA levels were measured by q-PCR. **e** Cellular protein was extracted and target protein (MST1, AMPK, SREBP-1c, ACC, and FAS) expression was determined by immunoblotting using commercially available antibodies. The relative protein expression was quantified by densitometry and normalized to β -actin expression level. **f** mRNA expression was determined by q-PCR. The relative gene expression was normalized to GAPDH levels. Data are expressed as the mean \pm SEM ($n=3$). * $p<0.05$, ** $p<0.01$, *** $p<0.001$

were associated with the aggravated hepatic lipogenesis and reduction in lipolysis, possibly through regulation of SREBP-1c and AMPK pathway. Importantly, MST1 expression reverses the miR-199a-5p stimulated lipid accumulation in AML-12 cells, which provide direct evidence that miR-199-5p may function through MST1 in modulation of hepatic lipid metabolism.

An earlier study reported that miR-199a-5p is associated with the progression of liver fibrosis in human patients [39]. miR-199a-5p expression significantly upregulated the fibrosis related gene expression (metalloproteinases-1, a1 procollagen, MMP13), an effect attributed to the regulation of the target genes on the TGF β signaling pathway [39]. Recent study further confirmed that miR-199a was significantly upregulated in CCl4 induced liver fibrosis mouse/ rat model and human cirrhosis patients [40]. Moreover, overexpression of miR-199a markedly enhances the expression of fibrosis marker (fibronectin, connective tissue growth factor and α -smooth muscle actin) in rat liver cells, by suppressing caveolin 2 and the subsequent stimulating of TGF β signaling pathway [40]. Another study demonstrated that miR-199a-5p was significantly upregulated in NAFLD patients and steatosis mouse model. miR-199a-5p stimulated the progression of steatosis through inhibiting caveolin 1 and PPAR α signaling, which subsequently suppresses mitochondrial-related fatty acid beta oxidation [41].

In normal condition, on the basis of the the high-throughput small RNA sequencing (sRNA-seq), the expression level of miR-199a-5p in liver is relatively low. However, the miR-199-5p expression is markedly elevated in NAFLD mouse models and human NAFLD patients. Interestingly, the most abundant miR-199a-5p was expressed in adipose tissue and its expression level was upregulated in NAFLD mouse models. According to the recent study, adipose-derived miRNAs can travel through circulation and modulate target gene expression in other tissues [25]. This was a novel endocrine regulation way which is supposed to be far superior to what had been previously thought. Exosomes, identified as effective carriers of miRNA to distant cells and tissues, have been shown to stabilize miRNA [16, 42]. It is possible

that adipose tissue derived miR-199a-5p, could be delivered to the liver via circulation by exosomes, and directly modulates the hepatic lipid metabolism. Such hypothesis had been confirmed by the current study which showed miRNA-containing exosomes (EXO-miR) by a vector that specifically encapsulates miRNA-199a-5p are capable of transporting miRNA-199a-5p to targeted cells in liver tissues. Importantly, these EXO-miR-199a-5p delivered to liver was capable of modulating hepatic lipid accumulation in NAFLD mouse model.

Further exploration of the molecular mechanism of miR-199a-5p in hepatic lipid metabolism identified MST1 as the target gene of miR-199a-5p. EXO-miR-199a expression is inversely correlated with MST1 expression in NAFLD model and dual luciferase assay further revealed MST1 as a novel target gene for miR-199a-5p. MST1 has been reported to exert protective effects against NAFLD through targeting SREBP and the Sirt1 ubiquitination [33]. In line with previous report, our results also showed that MST1 is inversely correlated with hepatic lipid accumulation in both NAFLD mouse model and patients. Furthermore, overexpression of MST1 in the liver stimulates the phosphorylation of AMPK, with subsequent increase of CPT-1 α expression, thus accelerates liver fat oxidation. In addition, we also found that MST1 can inhibit the expression of FASN, reduce the rate of fat synthesis.

In addition, recent studies indicate that the apoptosis and autophagy pathways impact the initiation and progression of NAFLD and NASH [43–45]. Previous studies reported miR-199a-5p-induced cancer cell apoptosis by targeting on Mixed Lineage Kinase 3/NF κ B [46]. Moreover, in cardiomyocytes, miR-199a-5p impaired autophagy process through activation of mTOR/GSK3 β signaling and inhibition of the Atg5, LC3B as well as BECN1 expression [47]. Thereby, miR-199a-5p might also exert important roles in hepatocyte/ Kupfer cell apoptosis and autophagy pathways in the disease process of NAFLD/NASH. The impact of miR-199a-5p in these important pathways in the disease process of NAFLD/ NASH warrants further investigation in the future studies.

With the increasing endocrine function of adipose tissue, adipose tissue crosstalk between liver tissue has also aroused widespread interest. It has been reported that adipose tissue is the main source of circulating miRNAs which have been reported to have important regulatory effects on hepatic lipid metabolism, including miR-122, miR-24, miR-370, miR-378/378, miR-335, miR-125a-5p, miR-33a/33b [48–51]. Dysregulation of miRNAs may directly contribute to metabolic disorders, suggesting that miRNAs may potentially be used as therapeutic targets for metabolic diseases.

In summary, our data demonstrate for the first time that miR-199a-5p contributes to the development of NAFLD, possibly through the regulation of the target MST1 expression. miR-199a, which is highly expressed in adipose

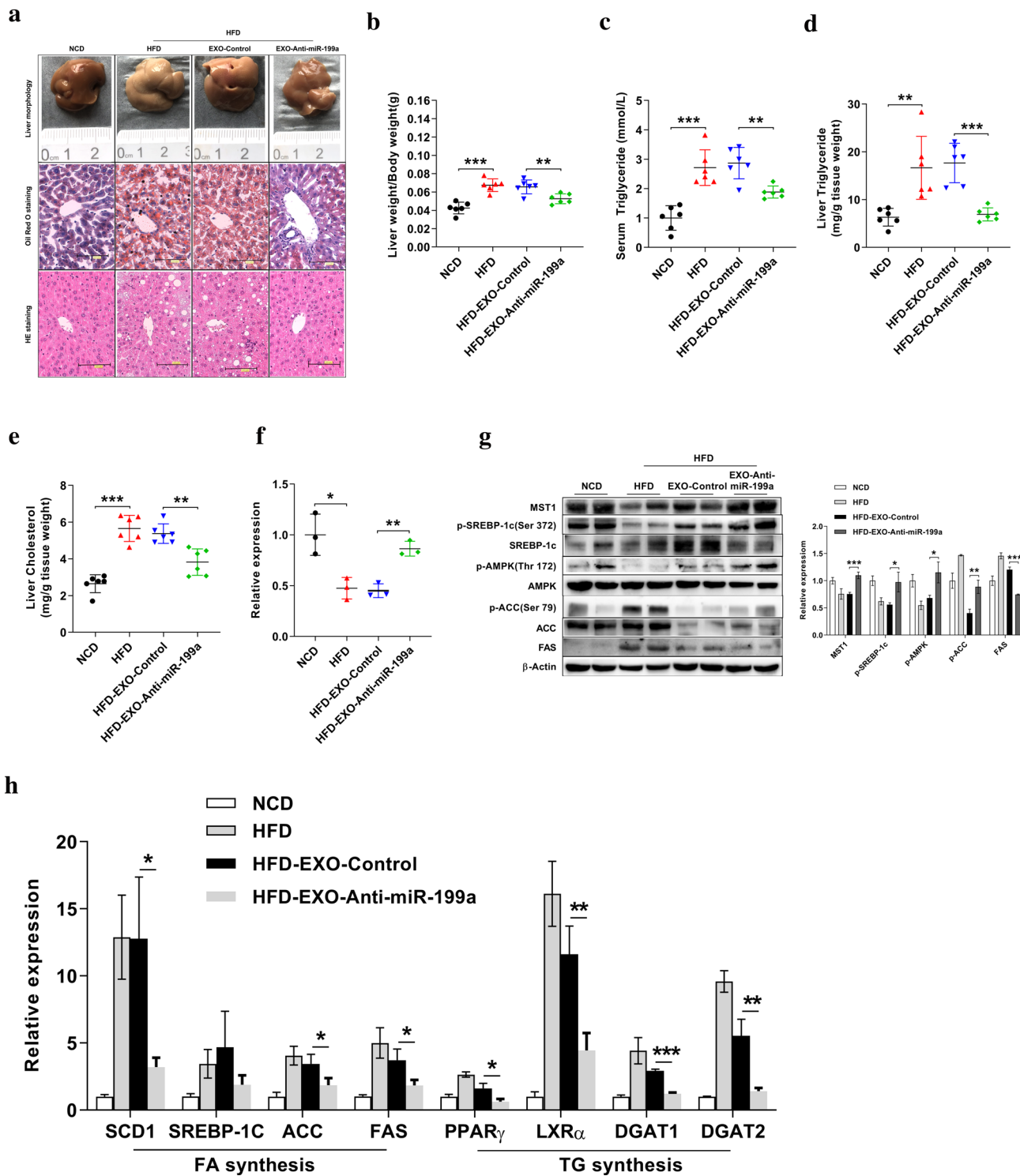


Fig. 7 EXO-miR-199a inhibitor inhibits fat accumulation in vivo. (A-H). Mice were fed on NCD or HFD for 12 weeks, which HFD mice were injected through the tail vein with 30 μ g exosomes containing either negative control or anti-miR-199a bi-weekly for three additional weeks. Mice were taken down and blood and liver were collected. **a** Representative images of liver sections stained with ORO and H&E staining. Scale bar 100 μ m. **b** Fresh liver weight ($n=6$). **c-e** Plasma and liver lipid contents as determined by commercially available kits ($n=6$). **c** Plasma TG levels. **d** Liver TG levels. **e** Liver cholesterol levels. Hepatic MST1 mRNA level. The mRNA levels were measured by q-PCR ($n=3$). **g** Immunoblotting analysis of target protein expression using commercially available antibodies. The relative expression was determined by densitometry and normalized to β -actin levels. **h** mRNA levels were measured by q-PCR and normalized to GAPDH levels. Data are expressed as the mean \pm SEM ($n=8$). * $p<0.05$, ** $p<0.01$, *** $p<0.001$

available kits ($n=6$). **c** Plasma TG levels. **d** Liver TG levels. **e** Liver cholesterol levels. Hepatic MST1 mRNA level. The mRNA levels were measured by q-PCR ($n=3$). **g** Immunoblotting analysis of target protein expression using commercially available antibodies. The relative expression was determined by densitometry and normalized to β -actin levels. **h** mRNA levels were measured by q-PCR and normalized to GAPDH levels. Data are expressed as the mean \pm SEM ($n=8$). * $p<0.05$, ** $p<0.01$, *** $p<0.001$

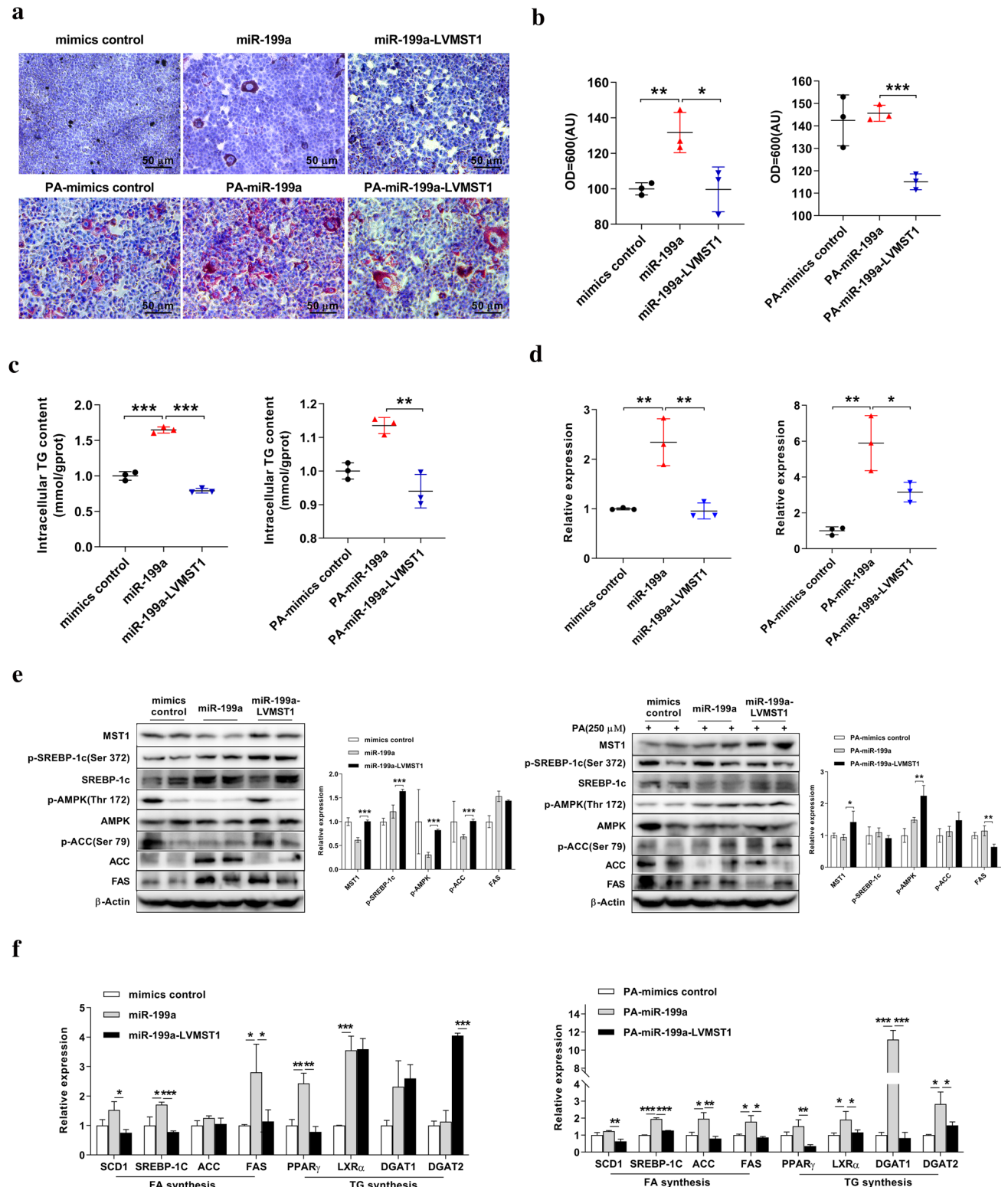
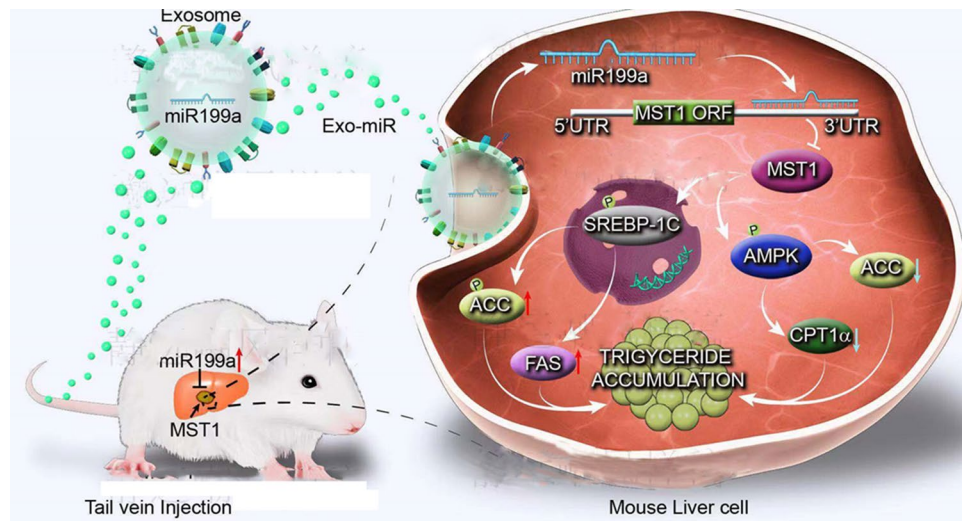


Fig. 8 Overexpression of MST1 reverse miR-199a-5p-induced hepatic steatosis. **a-f** AML-12 cells transfected with miR-199a-5p in the absence or presence of PA. After 48 h, cells were transfected with MST1 lentiviral vector for additional 24 h. Cellular lipid accumulation was determined by ORO staining (**a, b**) and intracellular TG content (**c**). **d** MST1 mRNA levels were measured by q-PCR. **e**

Immunoblotting analysis of target protein expression using commercially available antibodies. The relative expression was determined by densitometry and normalized to β -actin levels. **f** The mRNA levels of lipid-related genes were measured by q-PCR and normalized to GAPDH. Data are expressed as the mean \pm SEM ($n=3$). * $p < 0.05$, ** $p < 0.01$, *** $p < 0.001$. Scale bar 50 μ m

Fig. 9 Exosomal miR-199a-5p promotes hepatic lipid accumulation by targeting MST1 pathway. Delivery of miR-199a-5p with exosomes into mice aggravated liver lipid accumulation in hepatocytes, accompanied by down-regulation of hepatic MST1 expression. Inhibition of MST1 expression further modulates hepatic SREBP-1c and AMPK signaling cascades which subsequently impact CPT1 α and FASN (essential enzymes for lipolysis and lipogenesis)



tissue, can be successfully delivered to the target tissue through exosomes. Overexpression of miR-199a-5p led to a down-regulation of hepatic MST1, resulting in alteration in AMPK/SREBP1c signaling cascades, which subsequently impact CPT1 α and FAS, essential enzymes for lipolysis and lipogenesis. Ultimately, stimulate the lipid accumulation in the liver (Fig. 8). Therefore, antagonist to the miR-199a-5p might be a potential therapeutic approach against NAFLD. Given the fact that miR-199-5p level was drastically elevated in NAFLD mouse model and NAFLD patients, miR-199-5p might also serve as a potential marker for the diagnosis of NAFLD/NASH, which warrants further analysis in the future study.

Acknowledgements This work was supported by the following funding source: Y. Yang: National Natural Science Foundation of China (Nos. 81670798 and 81460166) the spring plan of Ministry of Education (Z2016039), West China Top Class Discipline Project in Basic Medical Sciences, Ningxia Medical University. Z.W. Yang : Chinese Academy of Medical Sciences Innovation Fund for Medical Sciences (CIFMS, 2016-I2M-1-016). X. Wu: National Natural Science Foundation of China (NSFC) (81800402); Central University Basic Research Business Fees of Peking Union Medical College, 333201810

Author contributions YY, LC, and YHL designed the study. YHL and YSL conducted the experiments. JNL, YL, HS, and YHY analyzed the data. HQ and XXW performed the animal experiments. YY, LC, and YHL wrote and edited the paper. ZWY provided essential experimental materials and molecular biology techniques. All authors reviewed the paper and approved the submitted and published versions of the paper.

Compliance with ethical standards

Conflict of interest Yuhan Li, Yansong Luan, Jianning Li, Hui Song, Yan Li, Hi Qi, Bo Sun, Peng Zhang, Xianxian Wu, Xing Liu, Yanhui Yang, Wufan Tao, Lei Cai, Zhiwei Yang, Yi Yang declare that they have no conflict of interest.

Ethical approval The collection of these human liver specimens was performed in accordance with the Ethical Committee on Human Research of the participating hospitals. All the patients were informed of the usage of the samples and written consent forms were obtained prior to the initiation of the study. Then mice were injected through the tail vein with 30 μ g exosomes containing either a negative control (miR-NT) or miRNA mimics (miR-199a) and NC inhibitor or miRNA inhibitor (anti-miR-199a) bi-weekly for 3 weeks. All animal procedures were conducted according to the protocols approved by the Committee of Animal Use for Research and Teaching of Ningxia Medical University, Yinchuan, China (SCXK (Ning) 2015-0001).

References

- Loomba R, Sanyal AJ. The global NAFLD epidemic. *Nat Rev Gastroenterol Hepatol*. 2013;10:686–90.
- Musso G, Cassader M, Gambino R. Non-alcoholic steatohepatitis: emerging molecular targets and therapeutic strategies. *Nat Rev Drug Discov*. 2016;15:249–74.
- Hardy T, Mann DA. Epigenetics in liver disease: from biology to therapeutics. *Gut*. 2016;65:1895–905.
- Stender S, Kozlitina J, Nordestgaard BG, Tybjaerg-Hansen A, Hobbs HH, Cohen JC. Adiposity amplifies the genetic risk of fatty liver disease conferred by multiple loci. *Nat Genet*. 2017;49:842–7.
- Zhang X, Ji X, Wang Q, Li JZ. New insight into inter-organ cross-talk contributing to the pathogenesis of non-alcoholic fatty liver disease (NAFLD). *Protein Cell*. 2018;9:164–77.
- Wree A, Broderick L, Canbay A, Hoffman HM, Feldstein AE. From NAFLD to NASH to cirrhosis-new insights into disease mechanisms. *Nat Rev Gastroenterol Hepatol*. 2013;10:627–36.
- Korf H, van der Merwe S. Adipose-derived exosomal MicroRNAs orchestrate gene regulation in the liver: Is this the missing link in nonalcoholic fatty liver disease? *Hepatology*. 2017;66:1689–91.
- Chalasani N, Younossi Z, Lavine JE, Diehl AM, Brunt EM, Cusi K, Charlton M, et al. The diagnosis and management of non-alcoholic fatty liver disease: practice guideline by the American Association for the Study of Liver Diseases, American College

- of Gastroenterology, and the American Gastroenterological Association. *Am J Gastroenterol.* 2012;107:811–26.
9. Ahmed A, Wong RJ, Harrison SA. Nonalcoholic fatty liver disease review: diagnosis, treatment, and outcomes. *Clin Gastroenterol Hepatol.* 2015;13:2062–70.
 10. Monetti M, Levin MC, Watt MJ, Sajan MP, Marmor S, Hubbard BK, Stevens RD, et al. Dissociation of hepatic steatosis and insulin resistance in mice overexpressing DGAT in the liver. *Cell Metab.* 2007;6:69–78.
 11. Goedeke L, Bates J, Vatner DF, Perry RJ, Wang T, Ramirez R, Li L, et al. Acetyl-CoA carboxylase inhibition reverses NAFLD and hepatic insulin resistance but promotes hypertriglyceridemia in rodents. *Hepatology.* 2018;68:2197–211.
 12. Li Y, Xu S, Mihaylova MM, Zheng B, Hou X, Jiang B, Park O, et al. AMPK phosphorylates and inhibits SREBP activity to attenuate hepatic steatosis and atherosclerosis in diet-induced insulin-resistant mice. *Cell Metab.* 2011;13:376–88.
 13. Krol J, Loedige I, Filipowicz W. The widespread regulation of microRNA biogenesis, function and decay. *Nat Rev Genet.* 2010;11:597–610.
 14. Bartel DP. MicroRNAs: target recognition and regulatory functions. *Cell.* 2009;136:215–33.
 15. Jonas S, Izaurralde E. Towards a molecular understanding of microRNA-mediated gene silencing. *Nat Rev Genet.* 2015;16:421–33.
 16. Zhang L, Zhang S, Yao J, Lowery FJ, Zhang Q, Huang WC, Li P, et al. Microenvironment-induced PTEN loss by exosomal microRNA primes brain metastasis outgrowth. *Nature.* 2015;527:100–4.
 17. Mayourian J, Ceholski DK, Gorski PA, Mathiyalagan P, Murphy JF, Salazar SI, Stillitano F, et al. Exosomal microRNA-21-5p mediates mesenchymal stem cell paracrine effects on human cardiac tissue contractility. *Circ Res.* 2018;122:933–44.
 18. Valadi H, Ekstrom K, Bossios A, Sjostrand M, Lee JJ, Lotvall JO. Exosome-mediated transfer of mRNAs and microRNAs is a novel mechanism of genetic exchange between cells. *Nat Cell Biol.* 2007;9:654–9.
 19. Raposo G, Stoorvogel W. Extracellular vesicles: exosomes, microvesicles, and friends. *J Cell Biol.* 2013;200:373–83.
 20. Wang X, Wang H, Cao J, Ye C. Exosomes from adipose-derived stem cells promotes VEGF-C-dependent lymphangiogenesis by regulating miRNA-132/TGF-beta pathway. *Cell Physiol Biochem.* 2018;49:160–71.
 21. Ferrante SC, Nadler EP, Pillai DK, Hubal MJ, Wang Z, Wang JM, Gordish-Dressman H, et al. Adipocyte-derived exosomal miRNAs: a novel mechanism for obesity-related disease. *Pediatr Res.* 2015;77:447–54.
 22. Maas SLN, Breakfield XO, Weaver AM. Extracellular vesicles: unique intercellular delivery vehicles. *Trends Cell Biol.* 2017;27:172–88.
 23. Mori MA, Raghavan P, Thomou T, Boucher J, Robida-Stubbs S, Macotela Y, Russell SJ, et al. Role of microRNA processing in adipose tissue in stress defense and longevity. *Cell Metab.* 2012;16:336–47.
 24. Ying W, Riopel M, Bandyopadhyay G, Dong Y, Birmingham A, Seo JB, Ofrecio JM, et al. Adipose tissue macrophage-derived exosomal miRNAs can modulate in vivo and in vitro insulin sensitivity. *Cell.* 2017;171(372–384):e312.
 25. Thomou T, Mori MA, Dreyfuss JM, Konishi M, Sakaguchi M, Wolfrum C, Rao TN, et al. Adipose-derived circulating miRNAs regulate gene expression in other tissues. *Nature.* 2017;542:450–5.
 26. Kim S, Lee UJ, Kim MN, Lee EJ, Kim JY, Lee MY, Choung S, et al. MicroRNA miR-199a* regulates the MET proto-oncogene and the downstream extracellular signal-regulated kinase 2 (ERK2). *J Biol Chem.* 2008;283:18158–66.
 27. Shatseva T, Lee DY, Deng Z, Yang BB. MicroRNA miR-199a-3p regulates cell proliferation and survival by targeting caveolin-2. *J Cell Sci.* 2011;124:2826–36.
 28. Wang Z, Ma X, Cai Q, Wang X, Yu B, Cai Q, Liu B, et al. MiR-199a-3p promotes gastric cancer progression by targeting ZHX1. *FEBS Lett.* 2014;588:4504–12.
 29. Qu Y, Huang X, Li Z, Liu J, Wu J, Chen D, Zhao F, et al. miR-199a-3p inhibits aurora kinase A and attenuates prostate cancer growth: new avenue for prostate cancer treatment. *Am J Pathol.* 2014;184:1541–9.
 30. Ren K, Li T, Zhang W, Ren J, Li Z, Wu G. miR-199a-3p inhibits cell proliferation and induces apoptosis by targeting YAP1, suppressing Jagged1-Notch signaling in human hepatocellular carcinoma. *J Biomed Sci.* 2016;23:79.
 31. Gu N, You L, Shi C, Yang L, Pang L, Cui X, Ji C, et al. Expression of miR-199a-3p in human adipocytes is regulated by free fatty acids and adipokines. *Mol Med Rep.* 2016;14:1180–6.
 32. Zhang M, Zhang L, Hu J, Lin J, Wang T, Duan Y, Man W, et al. MST1 coordinately regulates autophagy and apoptosis in diabetic cardiomyopathy in mice. *Diabetologia.* 2016;59:2435–47.
 33. Geng C, Zhang Y, Gao Y, Tao W, Zhang H, Liu X, Fang F, et al. Mst1 regulates hepatic lipid metabolism by inhibiting Sirt1 ubiquitination in mice. *Biochem Biophys Res Commun.* 2016;471:444–9.
 34. Ardestani A, Paroni F, Azizi Z, Kaur S, Khobragade V, Yuan T, Frogne T, et al. MST1 is a key regulator of beta cell apoptosis and dysfunction in diabetes. *Nat Med.* 2014;20:385–97.
 35. Jeong SH, Kim HB, Kim MC, Lee JM, Lee JH, Kim JH, Kim JW, et al. Hippo-mediated suppression of IRS2/AKT signaling prevents hepatic steatosis and liver cancer. *J Clin Invest.* 2018;128:1010–25.
 36. Park BH, Kim DS, Won GW, Jeon HJ, Oh BC, Lee Y, Kim EG, et al. Mammalian ste20-like kinase and SAV1 promote 3T3-L1 adipocyte differentiation by activation of PPARgamma. *PLoS ONE.* 2012;7:e30983.
 37. Nascimbeni F, Bedossa P, Fedchuk L, Pais R, Charlotte F, Lebray P, Poynard T, et al. Clinical validation of the FLIP algorithm and the SAF score in patients with non-alcoholic fatty liver disease. *J Hepatol.* 2020;72:828–38.
 38. Bedossa P, Consortium FP (2014) Utility and appropriateness of the fatty liver inhibition of progression (FLIP) algorithm and steatosis, activity, and fibrosis (SAF) score in the evaluation of biopsies of nonalcoholic fatty liver disease. *Hepatology* 60:565–575.
 39. Murakami Y, Toyoda H, Tanaka M, Kuroda M, Harada Y, Matsuda F, Tajima A, et al. The progression of liver fibrosis is related with overexpression of the miR-199 and 200 families. *PLoS ONE.* 2011;6:e16081.
 40. Yang X, Ma L, Wei R, Ye T, Zhou J, Wen M, Men R, et al. Twist1-induced miR-199a-3p promotes liver fibrosis by suppressing caveolin-2 and activating TGF-beta pathway. *Signal Transduct Target Ther.* 2020;5:75.
 41. Li B, Zhang Z, Zhang H, Quan K, Lu Y, Cai D, Ning G. Aberrant miR199a-5p/caveolin1/PPARalpha axis in hepatic steatosis. *J Mol Endocrinol.* 2014;53:393–403.
 42. Deng ZB, Poliakov A, Hardy RW, Clements R, Liu C, Liu Y, Wang J, et al. Adipose tissue exosome-like vesicles mediate activation of macrophage-induced insulin resistance. *Diabetes.* 2009;58:2498–505.
 43. Allaire M, Rautou PE, Codogno P, Lotersztajn S. Autophagy in liver diseases: time for translation? *J Hepatol.* 2019;70:985–98.
 44. Kanda T, Matsuoka S, Yamazaki M, Shibata T, Nirei K, Takahashi H, Kaneko T, et al. Apoptosis and non-alcoholic fatty liver diseases. *World J Gastroenterol.* 2018;24:2661–722.
 45. Arab JP, Arrese M, Trauner M. Recent insights into the pathogenesis of nonalcoholic fatty liver disease. *Annu Rev Pathol.* 2018;13:321–50.

46. Song T, Zhang X, Yang G, Song Y, Cai W. Decrement of miR-199a-5p contributes to the tumorigenesis of bladder urothelial carcinoma by regulating MLK3/NF-kappaB pathway. *Am J Transl Res.* 2015;7:2786–94.
47. Li Z, Song Y, Liu L, Hou N, An X, Zhan D, Li Y, et al. miR-199a impairs autophagy and induces cardiac hypertrophy through mTOR activation. *Cell Death Differ.* 2017;24:1205–13.
48. Lou G, Song X, Yang F, Wu S, Wang J, Chen Z, Liu Y. Exosomes derived from miR-122-modified adipose tissue-derived MSCs increase chemosensitivity of hepatocellular carcinoma. *J Hematol Oncol.* 2015;8:122.
49. Wang F, Li L, Piontek K, Sakaguchi M, Selaru FM. Exosome miR-335 as a novel therapeutic strategy in hepatocellular carcinoma. *Hepatology.* 2018;67:940–54.
50. Vega-Badillo J, Gutierrez-Vidal R, Hernandez-Perez HA, Vil-lamil-Ramirez H, Leon-Mimila P, Sanchez-Munoz F, Moran-Ramos S, et al. Hepatic miR-33a/miR-144 and their target gene ABCA1 are associated with steatohepatitis in morbidly obese subjects. *Liver Int.* 2016;36:1383–91.
51. Sulaiman SA, Muhsin NIA, Jamal R. Regulatory non-coding rnas network in non-alcoholic fatty liver disease. *Front Physiol.* 2019;10:279.

Publisher's Note Springer Nature remains neutral with regard to jurisdictional claims in published maps and institutional affiliations.